Integration of high-resolution, Active and Passive Remote Sensing in support to Tsunami Preparedness and Contingency Planning

Book Section

Integration of high-resolution, Active and Passive Remote Sensing in support to Tsunami Preparedness and Contingency Planning

Fabrizio Ferrucci
Università della Calabria Italy

1. Introduction

Known from time immemorial to the inhabitants of the Pacific region, tsunamis became worldwide known with the great Indian Ocean disaster of December 26, 2004, and its toll of about 234'000 deaths, 14'000 missing and over 2,000,000 displaced persons. Beyond triggering the international help in managing the immediate post-event, and sustaining eventual rehabilitation of about 10'000 km² of hit coastal areas, the disaster scenario was intensively focused on by spaceborne remote sensing. The latter, was the only fast and appropriate mean of collecting updated information in as much as 14 hit countries, stretching from Indonesia to South Africa across the Indian Ocean.

Short-term, institutional satellite observation response was mostly centered on the International Charter on Space and Major Disasters, a joint endeavor of 17 public and private satellite owners worldwide (including the three founding agencies: ESA-European Space Agency, CNES-Centre National d'Etudes Spatiales, and CCRS-Canadian Center for Remote Sensing) that provided emergency spaceborne imaging and rapid mapping support (www.disasterscharter.org/web/charter/activations).

In disaster response, remote sensing information needs are usually restrained to damage assessment, thus have limited duration. This implies that information must be timely and timely useable, and be provided with high-to-very high spatial resolution.

Conversely, high temporal resolution - useful in repeated damage assessment across moderate or long lasting events, as for example storm sequences, earthquake swarms and volcanic unrests - is generally unnecessary in the tsunami case, where damage presents large amplitude but is assessed once and for all after the main wavetrain has struck.

A much wider community of institutional and private users of remote sensing information, in form of special cartography products, and much longer lasting benefits are experienced if information is used for tsunami flooding risk mapping, impact scenario building and the inherent contingency planning.

Benefits are intimately connected to the characteristics of tsunamis that occur seldom, propagate at top speeds close to 200 m/s on deep ocean floors, and can hit in a few hours areas distant thousands of kilometers from the source. On account of these parameters, tsunami impact mitigation cannot simply rely upon response.

In 2004, once the earthquake originating the tsunami was felt, it would have been possible to give a 2-hour advance impact notice in distant countries as India, Sri Lanka and Maldives. This did not happen, because a monitoring-and-alert system as the current PTWC-Pacific Tsunami Warning Center managed by NOAA-National Ocean and Atmosphere Administration (www.prh.noaa.gov/ptwc/) did not exist yet in the Indian Ocean. However, since slowest velocities of tsunami waves are much larger than humans can run for escaping them, in lack of efficient emergency plans to enact immediately, it is clear that the alert system alone would not have solved the problem.
We can conclude that the risk can be mitigated acting principally on early warnings and preparedness. The latter is by far the leading issue, as preparedness measures can be effective even without early warning, whereas early warning is useless without accompanying measures.
Here, we discuss how a multi-technique, integrated remote sensing approach provides the essential information to satisfy prevention and response needs in a tsunami prone area, located in the heart of the theater of the great 2004 Indian Ocean tsunami.

2. Tsunamis and Storm Surges

Tsunamis are liquid gravitational waves that are triggered by sudden displacement of water bodies by co-seismic seafloor dislocation or underwater landslide mass push/pull. The speed (celerity) of tsunami waves is

$$V=\sqrt{\frac{g\lambda}{2\pi}\tanh\left(2\pi\frac{d}{\lambda}\right)} \tag{1}$$

with g the gravity acceleration, d the thickness of the water layer in meters and λ the wavelength. If the argument of the hyperbolic tangent is large with $d > \lambda/2$, equation (1) reduces to

$$V_{max} \approx \sqrt{\frac{g\lambda}{2\pi}} \tag{2}$$

whereas in shallow waters and $d < \lambda/20$, equation (1) becomes

$$V_{min} \approx \sqrt{gd} \tag{3}$$

On account of the steadily large ratio between wavelength and thickness of the water layer, the shallow water approximation of equation (3) applies generally.
The main parameter that discriminates tsunamis from swell, is wavelength: wind generated waves present near-constant wavelengths up to a few hundred meters, and periods between seconds and tens of seconds.
Conversely, a tsunami wave as in equation (2) travelling in a 4000m thick ocean water layer, locally reaches 200m/s with periods of 100-120 minutes (or wavelenghts of several hundred kilometers) and unnoticeable amplitude with respect to wavelength. When approaching the

shore ('shoaling') with velocity dropping below 20 m/s, wavelengths shorten to kilometers, and wave amplitudes increase (run-up) before penetrating coastal areas.
Outstanding wave heights are obtained as a combination of steep seafloor topographic gradient, and a short distance from the source. The worst documented such case occurred in the near field of a M_W=8.0 earthquake in 1946 at Unimak Island, Alaska, where the Scotch Cap lighthouse was flushed away by a 35-meter high wave.
Reportedly, wave heights for the great Indian Ocean tsunami of 26th December 2004, may have exceeded 15 m along northern Sumatra coasts (Geist et al., 2007). In Sri Lanka, about 2000 km away from the epicentre of the M_W=9.2±0.1 earthquake, largest wave heights may have exceeded 10 m in the East, whereas at least 5000 lives were taken by wavetrains not higher than 4 m, in the South and the Southwest of the island.

YEAR	DAMAGE AREA (SOURCE AREA)	SOURCE TYPE	CASUALTIES (approx.)
2004	Eastern and Central Indian Ocean (Sumatra)	Earthquake	240000
1991	Bangladesh, Chittagong (category-5 tropical cyclone)	Storm surge	138000
1970	Bangladesh (Bhola category-4 tropical cyclone)	Storm surge	500000
1908	southern Italy, Messina and Reggio Calabria	Earthquake	100000
1896	Honshu (off-Sanriku, Japan)	Earthquake	27000
1883	Indonesia, Sunda strait (Krakatau)	Volcanic eruption	35000
1868	South America Pacific coasts (Peru-Chile, Arica)	Earthquake	70000
1771	Japan, Ryukyu Islands	Earthquake	13000
1755	Portugal, Lisbon (Alentejo fault and Carrincho bank)	Earthquake	60000
1741	Japan, Oshima and Hokkaido (controversial amplitude)	Volcano landslide	2000-15000

Table 1. Top-10 deadly seawater floodings worldwide in the last three Centuries, in inverse temporal order. Most frequent tsunami triggers relate to earthquakes, either directly (co-seismic displacement) or indirectly (submarine landslides; Tinti *et al.,* 2005): in terms of ground floor dislocation alone, earthquake Magnitudes M_w<7 are not believed to trigger tsunamis. In tropical areas of strong cyclogenetic activity as the Bay of Bengal and the Gulf of Mexico, the combination of strong tropical storms and low topographic gradient of coastal areas, may lead to massive inland penetration of sea waters called 'storm surge'.

With little modifications, the above concepts may consistently apply to storm driven water surges, or 'storm surges', a threat provided with much higher repeat frequency (yearly) than tsunamis. Storm surges, typically associated to tropical cyclones, are a near-permanent elevation of the sealevel for the duration of the event, arising from the combination of extreme atmospheric pressure drop and push of the associated strong winds. Storm surges are common in tropical areas worldwide. Storm surges were responsible of the largest, flood related, mass casualty ever scored (in Bangladesh, Bengal Bay, 1970; ca. 500'000, see Table 1). In economic terms, the costliest tropical storm surge was that associated to hurricane Katrina, August 2005, with over 100 Billion USD of direct and indirect losses.

3. Rationale

As stated earlier, operational effectiveness in tsunami impact mitigation requires taking major preparedness measures to allow exposed populations moving fast to the closest safe area nearby. This solution may allow avoiding blanket evacuation of tsunami jeopardized

areas, that may imply permanent activity banning in large, critical portions of the territory, especially if the topografic gradient is very low (as in Sri Lanka and Bangladesh, e.g.) and small increase of water levels lead to deep inland flooding.
In terms of preparedness, this means that escape way solutions must be addressed well in advance. Considering that unnoticeably elevated areas close to the shoreline can be good, and sometimes unexpected escape places to single out, map and include in emergency plans, protection against tsunamis and timeliness of response require the advance drawing of quantitative impact scenarios.
Emergency cartography must be frequently updated to mirror the modifications with time in location and value of vulnerable elements (inhabitants, buildings and infrastructures). This calls for the use of fast, synoptic and high-to-very high resolution mapping technologies: a need that can be satisfied by airborne and spaceborne remote sensing only. These concepts drove the design and the carrying out in 2006 - upon request of the Government of Sri Lanka to the Italian Government - of a thorough field investigation aimed to ease, provide with quantitative grounds and speed-up the national emergency planning in tsunami-prone areas. The request addressed the need of drawing a realistic set of flooding scenarios for most of the coastal areas of the island, with special emphasis on settlements and infrastructures in the reach of a model tsunami or a model storm surge. The basic criteria of investigation were broadly inspired by the format of early risk assessment and scenario simulation in the reference cases of Northwest USA (Mendocino and Humboldt in northern California, Tacoma in Washington, e.g.).
This portion of the Pacific coast is subjected to frequent tsunami impact from local seismic sources in the unresting, undersea Mendocino fault zone (Oppenheimer et al., 1993), and is focused on by the US National Tsunami Hazard Mitigation Program (Lander et al., 1993; Eisner et al., 2001; Priest et al., 2001; Venturato et al., 2007).
Downstream to US NTHMP, US Geological Survey provided dissemination of impact maps, portraying different scenarios based on possible tsunami impacts heights, and listing the number of people that would be affected by tsunamis of 5m, 10m, and 15m height respectively, with elevation data based on the SRTM (Shuttle Radar Topography Mission) Digital Elevation Model. The latter, is available worldwide. It displays planimetric resolution of 90 meters and absolute vertical accuracy of 9.6m (mission specifications). In the case of Sri Lanka, these parameters were considered not sufficient for reaching the required level of horizontal and vertical resolution compatible with a terrain heterogeneous at all scales, densely vegetated, provided with scattered manufacts eventually hidden or partly covered by tropical vegetation, and displaying negligible topographic gradients as low as 1-2% over much of the coastal zones of interest.
The drawing of quantitative flooding scenarios required collecting the information needed for completing the following steps, at the suitable scale:
i) model tsunami (at sea, before impact): requires detailed 3D knowledge of the seabed, aimed to model and forecast, spot by spot, the wavetrain pattern, the energy distribution and the run-up before impact. On account of the expected wavelengths to deal with, the ideal working scale for accurate modelling was considered to lie between 1/10000 and 1/20000 within at least 10 km from the shoreline. In lack of such information, and on account of unfavorable time and cost implications of an ad-hoc campaign, it was decided to rely upon the existing, loose seafloor cartographies by NOAA and British Admiralty, and the few wave heights observed in December 2004 (Liu et al., 2005).

ii) Model flooding (on land, after impact): requires very high-resolution 3-D terrain model, to simulate the hydraulic behavior of flooded zones at scales of 1/5000 or better, and to draw the limits of the impact zone, the expected severity of the areal impacts and, if appropriate, the energy absorption on impacted manufacts. In brief, the risk model and the scenarios, to permit emergency deciders to plan evacuation and safety measures, and urban planners to adopt structural measures finalized to ease citizens' escape in case of alert. According to urban planners, this target requires ground resolutions in the order of 1 m, and elevation precisions in the order of 0.2+0.3 m to be achieved uniformly over large areas.
Since the 2004 tsunami losses concentrated in ocean-bound strips of variable width, up to observed maxima of as much as 8 km in the East of the island (Batticaloa), the width of coastal areas to map and model was fixed at 3 km in average.
This pointed to an expected 1800 km² to map in 3D, in very short times (maximum one month), and with the resolutions/precisions as above: such target - clearly out of reach for standard topography missions - could be achieved only with use of State-of-the-Art active and passive remote sensing techniques.
It was chosen to combine airborne LiDAR and Hyperspectral - for top 3D resolution and simultaneous confidence qualification of elevation data - and spaceborne RaDAR (Prati et al., 1994) with multispectral mapping (Hirn & Ferrucci, 2005, 2006), aimed to extend Digital Elevation Model building and thematic mapping, to the whole of the areas requested by the Sri Lankan Government via the Disaster Management Center in Colombo. As a good balance between high resolution needs and feasibility issues, operational costs and security issues, the inter-Government agreement converged on mapping in 3D and at high-to-very high resolution, a portion of the coastal areas hosting at least two-thirds of damage and casualties observed in 2004.
Overall, the island had suffered 34'000 casualties and has experienced - for various reasons - over 1'100'000 displaced persons, ca. 500'000 of of which directly related to the tsunami destruction. The percentage of tsunami affected coastal populations ranged from 35% in the northern coastal districts of Kilinochi, to 80% in the eastern districts of Mullaitivu and 78% in Ampara, whereas the southern districts of Galle, Matara, and Hambantota displayed about 20% impact, albeit with scattered pockets of severe damage. The location map and the survey plan are shown in Figure 1.

4. The HyperDEM campaign

Following establishment of the inter-Government agreement five months after the 2004 tsunami, the operational project "'HyperDEM - The precise Digital Elevation Model of the coastal areas of Sri Lanka", was launched early in September 2005.
The work was completed in summer 2006 after acquisition of an overall data volume of 2.7 TeraBytes. Upon completion of the work, the End Users - the Disaster Management Center and the Ministry of Disaster Management and Humanitarian Affairs - were provided with ca. 2'500 km² of Digital Elevation Models of the coastal areas (location maps in Figure 1)

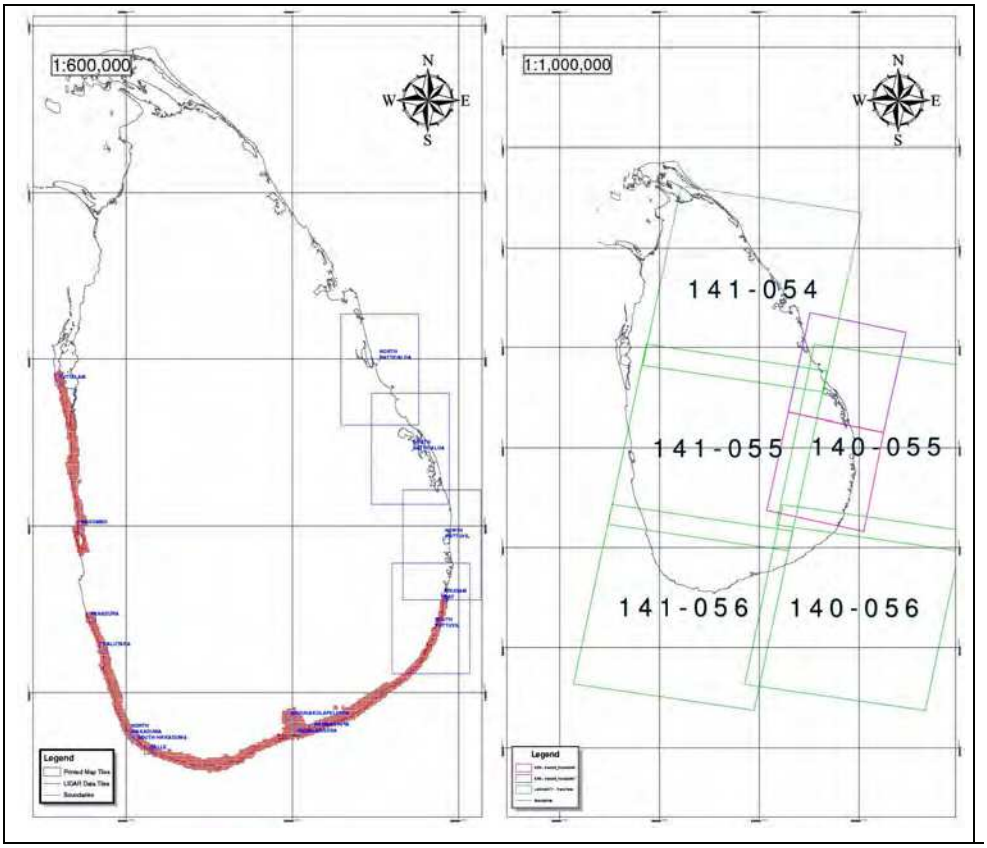

Fig. 1. (Left) Location map of areas surveyed by airborne LiDAR, hyperspectral and aerial photo (red squares) and spaceborne RaDAR (blue open squares). In the former, both Digital Elevation and Digital Surface Models were obtained at 1m resolution; in the latter, only DSM, at 30m resolution. (Right) Location of Landsat-7/ETM+ (green) and ERS-1 /ERS-2/ENVISAT (violet) satellite frames used in HyperDEM. ASTER and QuickBird imagery was also used for satisfying interpretation needs eventually arisen during processing of the 2.7 TeraByte dataset.

4.1 Airborne campaign

The airborne campaign and the related technical activities, were set up and carried out by the Istituto Nazionale di Oceanografia e Geofisica Sperimentale-OGS of Trieste, Italy. The survey, planned for integrated operation and combined acquisition of active and passive instruments at once, was designed on target ground resolutions of 1 m^2 for LiDAR (Figure 2), and 4 m^2 for hyperspectral (Figures 3, 4).

Fig. 2. Example of 3D rendering of combined LiDAR (1m planimetric resolution, 0.3 m precision in elevation on steady reflectors) and digital camera aerial scenery (resolution of 0.2 m). Picture taken over the artificial lake of Angunakolapelessa, north of Hambantota, south Sri Lanka.

After a long waiting because of a long lasting Autumn Monsoon, the survey was finally carried out in about one month after move-in of instruments to Colombo, early on February, 2006.

About 1'780 km² were LiDAR mapped airborne, at the planimetric resolution of 1 meter and the elevation precision of 0.3 metres (Figure 1, left), with the following payloads installed on the airborne platform, a De Havilland DHC-3 single-propeller "Otter" operated by the Sri Lankan private operator Air Taxi :

- a LiDAR system Optech ALTM 3033. The instrument consisted of a Near Infrared (A=1064 nm) Laser beam with pulse repetition rate of 33KHz. A scanning mirror directs the Laser optical pulses across the flight path, providing coverage to either sides of the flight direction. The forward motion of the aircraft provides coverage in the direction of flight.

ALTM 3033 incorporates a GPS receiver and an Inertial Measurement Unit (IMU), that acquires flight attitude data at the frequency of 200 Hz.

- A hyperspectral radiometer AISA Eagle 1K by the Finnish firm SPECIM. It is a pushbroom scanner made up of a V-NIR hyperspectral sensor, a GPS/INS Applanix sensor, and a laptop implemented data acquisition unit.

AISA Eagle 1K operates at wavelengths between 400-970 nm; it is able to record up to 244 bands (with spectral sampling of 2.3 nm/pixel) and 1024 spatial pixels. The system is flexible enough to allow acquiring data in almost every band combination, simultaneously acting on the number of bands and the bandwidth by use of a computer assisted procedure. We operated the system with 42-channel configuration, aimed at improving the signal-noise ratio in individual spectral bands.

- A semi-metric digital camera ROLLEI 6008 db45, with digital back Phase-One, model H2O. The camera presented a pixel spacing of 9 micrometers, in a scene composed of 4080 x 5440 pixel with 48-bit dynamics. Acquisition is assisted by a camera compensation system to adjust the roll and pitch variations due to aircraft position and flight attitude.

The decision to operate simultaneously the semi-metric digital camera with typical footprint in the order of 0.2 m (when operated at the same flight level useful in obtaining the nominal LiDAR resolution of 1 m) for assisting in the interpretation of ambiguous elevation features in the very-high resolution LiDAR and hyperspectral datasets.

In cartography applications, indeed, LiDAR raw elevation data are systematically purged of false or misleading information as those due to lateral backscattering, multiple scattering, returns from strongly reflecting physical surfaces, and so forth (Baltsavias, 1999; Kraus & Pfeifer, 1998).

Such information-cleaning process is performed through a classification process that allows assigning physical meaning to scatterers provided with variable signal/noise ratios. First pulses are typically associated to strongly reflecting objects, like trees, wires, roofs and bridges, whereas later (and weaker) pulses are attributed to returns from "ground" (Kraus & Pfeifer, 1998).

As stated earlier, the average inland extension of prospected area is about 3 km, with an isolated maximum of over 10 km in the sensitive area of the artificial basin and the dam of Angunakolapelessa (Figures 1-left and 2), immediate north of Hambantota in the south. Airborne LiDAR, orthophotos and hyperspectral data were acquired from February 11th and 21st, in two legs, separated by a four-day interval (17th to 20th February) devoted to process acquired data, assess the dataset completeness and plan eventual recoveries. The flight zone (Figure 1, left) spanned between Puttalam, in the West, and Pottuvil, in the Southeast. For security reasons, authorized flight plans did not include the capital, Colombo, nor some specific damaged coastal zones in the East (Trincomalee, Batticaloa, Ampara). Instead, eastern areas (Figure 1) were covered by spaceborne RaDAR, and qualified by high resolution spaceborne multispectral observation (Figure 1, right). Flight heights ranged between 900-2700 metres, as a function of the desired ground resolution, the morphology and land-cover of surveyed areas, and the meteorological conditions.

Flight paths were computed in real time by DGPS (differential kinematic GPS), using data simultaneously acquired by one GPS receiver onboard the aircraft and two, twin-frequency geodetic GPS receivers Ashtech (mod. Z-Extreme) at the fixed rate of one measurement per second. Twin-frequency GPS receivers were operated only on the benchmarks of an ad-hoc geodetic frame created by OGS, starting from a re-calculated benchmark of the Sri Lanka Survey Department, at the Katunayake International airport, north of Colombo.

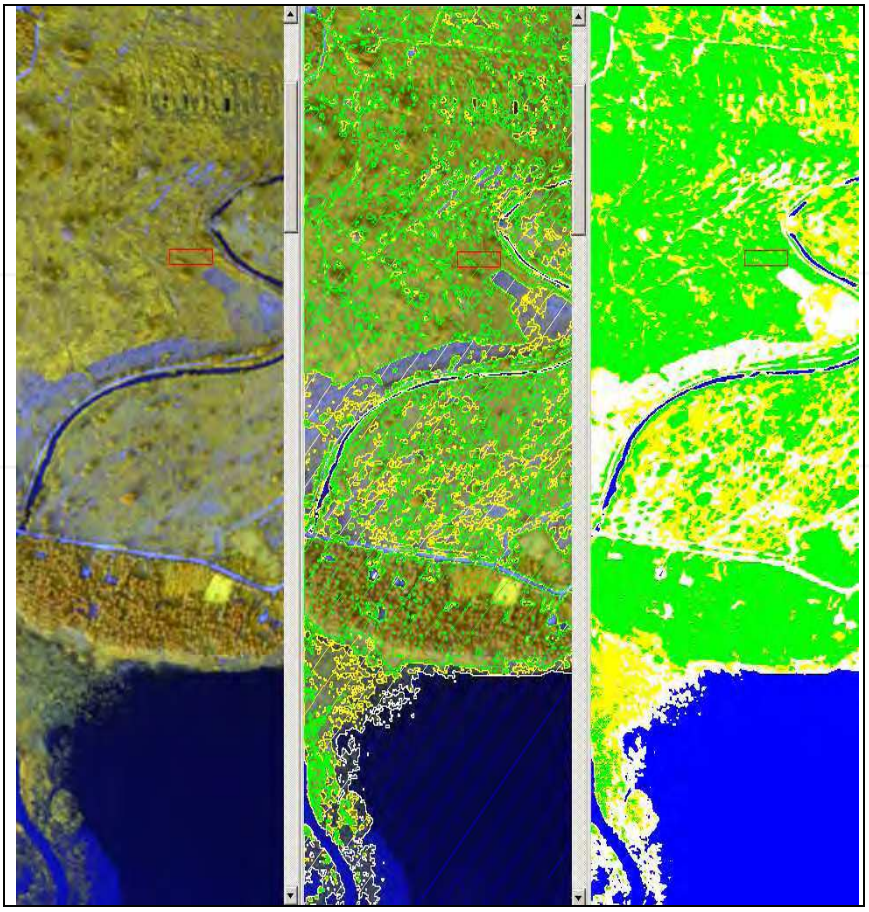

Fig. 3. Automated identification and contouring of 4x4 m² pixels unprovided with vegetation, done on AISA hyperspectral V-NIR data by use of a patented method, mutuated by burn scar analysis (Ferrucci & Hirn, 2005). Processing was conducted on raw data (left), aimed to prepare and carry out future operations in real-time. In contoured pixels (center), LiDAR elevation measurement are expected to be precise within the error estimate (±0.15m averaged over buildings and bare soils). Unlike vegetation, bare rocks, soils and buildings are the essential constituents of DSMs (see Figure 5) for flooding and tsunami impact simulation. The Level-2 classification (right) was used for pixel-by-pixel elevation quality assessment (Figure 4).

All benchmarks of the new geodetic frame were calculated and located on ellipsoids WGS84 and Everest 1830 in the Transverse Mercator projection. Upon completion of the campaign, the Sri Lanka Survey Dept. was provided with the monographs of newly established benchmarks.

The best estimate aircraft trajectory (SBET), made up of fixes spaced 0.15 cm in average, presented rms residual errors < 0.3m, that are compatible with the required precision in

elevation. Range data were geo-referenced by use of spatial and orientation parameters; basic products are vectors of points, including the information on position, GPS time and backscattered LiDAR amplitude. All products were delivered in UTM-44N projection, WGS84 datum.

Fig. 4. Sample output of the automated identification and contouring process of buildings and vegetation, done on 56-channel AISA hyperspectral VNIR data by use of a patented method, mutuated by burn scar analysis (Ferrucci & Hirn, 2005). In these pixels, LiDAR elevation measurement are expected to be precise within the error estimate (±0.15m averaged over buildings and bare soils).

Finally, bare pixels (without vegetation) were weighted 1, vegetated pixels weighted 0, and vegetated pixels for which two LiDAR returns are available (an early reflection from the top of canopy, and a late reflection from the underlying ground) were marked 0.5. This procedure allowed creating automatically (i) a mask including all points whose elevation is fully reliable within the nominal error range (Figure 4), and (ii) a three-dimensional, Level-2 land-cover of subsets weighted 0.5 and 1.

The information was completed by carrying out same bare soil classification on multispectral, very high-resolution, pre-/post-tsunami QuickBird data. In spite of the comparable pixel footprint, however, the 4-band Visible/Near-Infrared spectral content of QuickBird provided much poorer information than the airborne 56-band Hyperspectral airborne radiometer.

LiDAR data were also corrected by use of a geodic model derived from the EGM96 model. In particular, Digital Elevation Models obtained by airborne LiDAR, were associated to co-registered airborne Hyperspectral data that underwent unsupervised, Level-2 classification for automatically discriminating bare soil from vegetation.

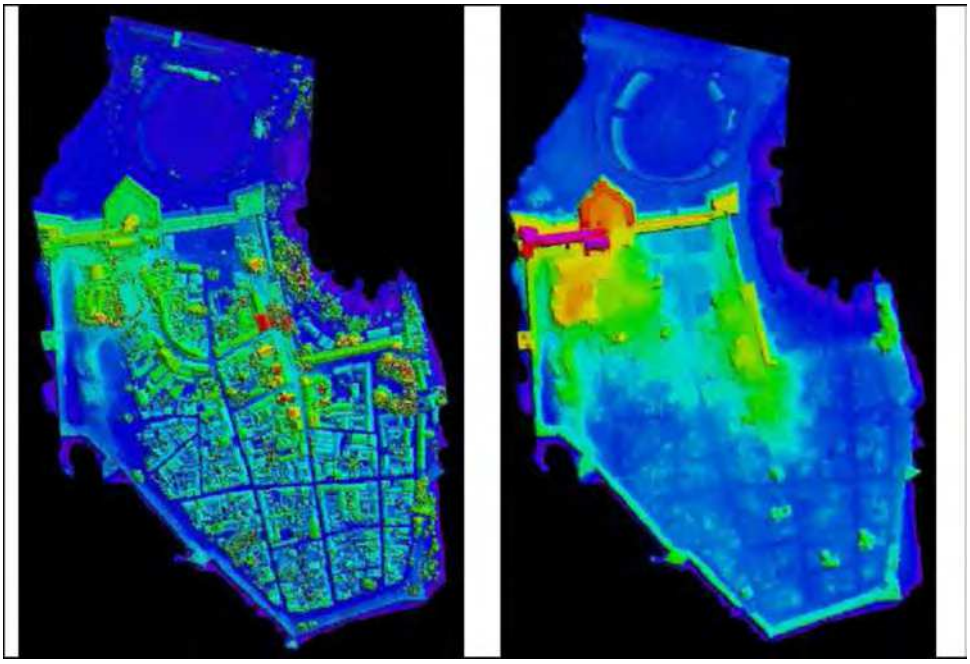

Fig. 5. LiDAR-derived Digital Surface Model (DSM, left) and Digital Ground Model (DGM, right). In the DGM, thick walls are emphasized by removal of most of buildings and vegetation. Because of such removal, DGMs are suited to standard cartography, but they are not to tsunami or storm surge flood modelling since they do not contain anymore relevant obstacles and vulnerable structures. The example relates to the 17th Century Dutch fort in Galle, southern Sri Lanka.

4.2 Spaceborne campaign

The spaceborne campaign was conducted synergetically by the Department of Electronics and Information of the Politecnico di Milano, that manufactured products in Synthetic Aperture Radar interferometry with the proprietary procedure PS-InSAR™ (Prati et al., 1994; Ferretti et al., 1999, 2001), and the University of Calabria, that manufactured multispectral and cartography products exploiting the proprietary procedure MyME2 (Hirn & Ferrucci, 2005; Ferrucci & Hirn, 2005).

The overall process relied upon same strategy as in the air campaign, with elevation data founded upon interferometric Synthetic Aperture RaDAR techniques, and pixel qualification carried out on Infra-Red multispectral satellite scenery.

Pixel qualification was based on the automated discrimination of bare soils, buildings and infrastructures from vegetation. These classes return highest confidence weight to RaDAR measured elevation values in the same pixel, whereas dense canopy returns lower or zero values. Overall, the space dataset was composed of 67 images, both RaDAR and multispectral, with resolutions ranging from metric (QuickBird) to decametric (ASTER, Landsat-7, ERS-1, ERS-2, Envisat). To fit the requirements of HyperDEM, repeat-pass interferometry was carried out to provide for two different products: Permanent Scatterers

(PS-InSAR™) data and DEM using ERS-1/ERS-2 'Tandem' pair combinations. PS-InSAR is a trademark of Politecnico di Milano.

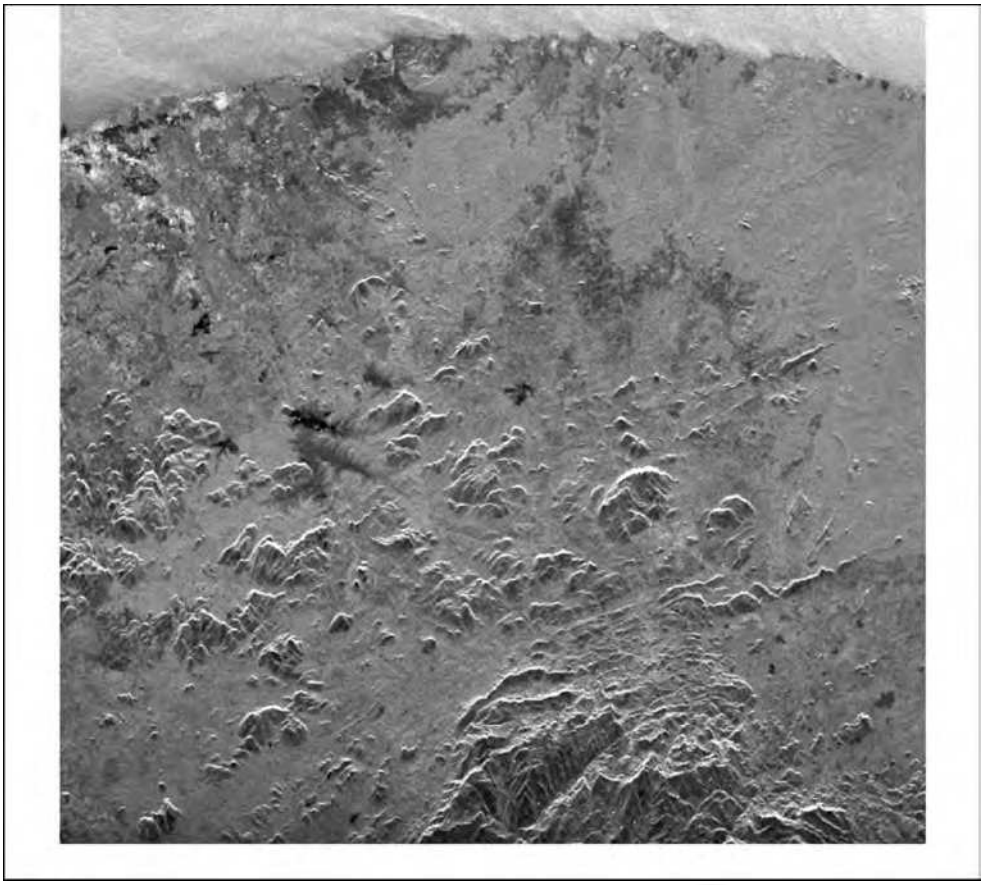

Fig. 6. View of the eastern coast (North is to the left) from radar satellites ERS (Track 33 - Frame 3465) of the European Space Agency. Because of the overall limited dataset, and the characteristics of the eastern coast areas (alternating rain forest, extremely flat terrains and frequent water bodies), the technical choice switched from PS-InSAR™ to Multi-Baseline InSAR technique.

The available SAR dataset was composed of 23 scenes along ERS/Envisat track 33 (Descending orbit), frames 3447 and 3465, acquired since 1992 at uneven rates. Accounting for the pixel dimensions (20m x 20m), and the lack of penetration of C-band RaDAR radiation across canopy, the elevation model mirrors the envelope of the Earth surface, including vegetation. In particular, the characteristics of the land cover make this area very sensitive to temporal decorrelation, that is, the loss of coherence between two successive images due to a large time interval elapsed between acquisitions. For this reasons, basic

RaDAR analysis was recentred on past ERS-1/ERS-2 tandem pairs, with 1-day intervals between over passes and 35-day repeat times.

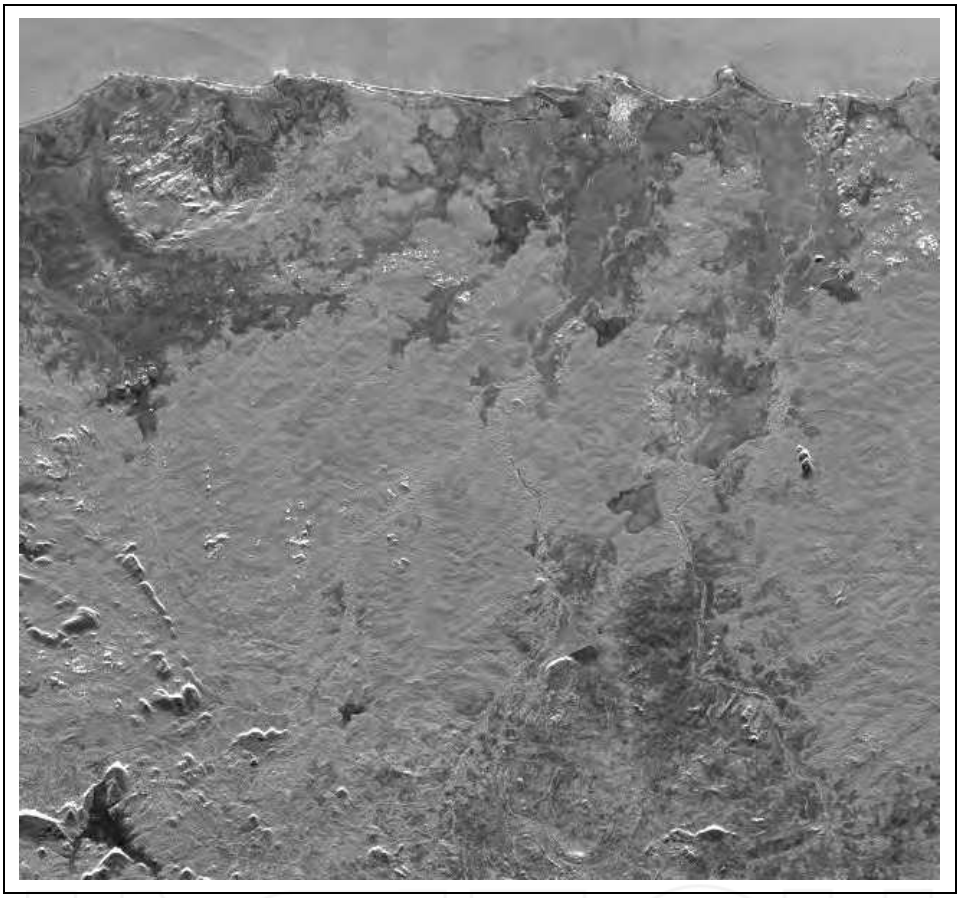

Fig. 7. SAR Multi-image, reflectivity map of a portion of the eastern coast of Sri Lanka (North is to the left). Dark shading indicates dense vegetation cover, whereas black areas correspond to internal water bodies. Radar scattering is de-organized by foliage, and water bodies favor forward scattering instead of backscattering towards the Radar platform. Both features in combination give rise to incoherent behaviour within multi-temporal sequences.

The useable SAR dataset, composed of 42 scenes, was theoretically sufficient for carrying out thorough PS-InSAR analysis. Conversely, the characteristics of land cover - in combination with the characteristics specified above of Synthetic Aperture RaDARs onboard the ESA spacecrafts - did not reveal suitable for thorough, Permanent Scatterer analysis (Figures 6, 7).
After elimination of tandem pairs with baseline larger than 1km, only 5 pairs for frame 3465, and only 3 for frame 3447 were left. This forced moving from the PS-InSAR™ technique to

the Multi-Interferogram approach (Prati et al., 1994; Ferretti et al., 1999): which is less precise, but less sensitive to the quantity of data (Figure 8).

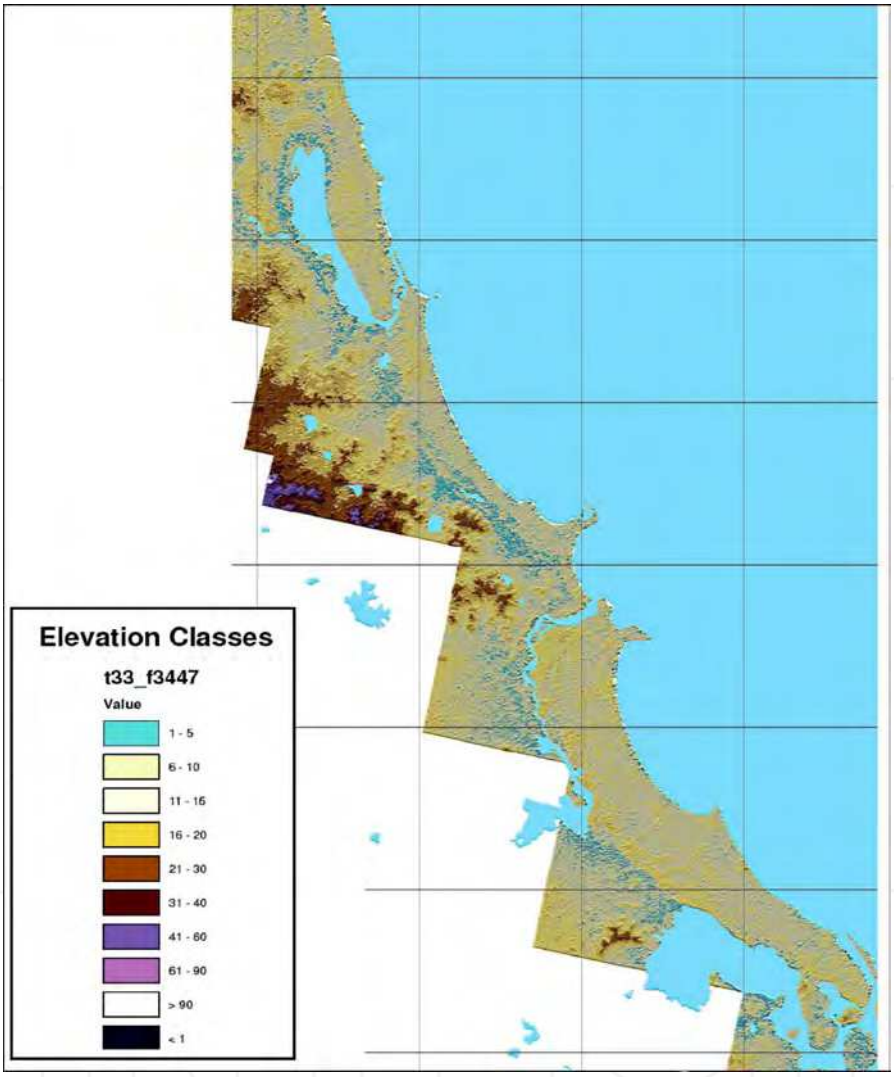

Fig. 8. Multi-interferogram DSM of eastern Sri Lanka: particular of the area of Batticaloa. Legend of elevation classes witnesses of a very flat topography that, with rich vegetation cover and spatial frequence of water bodies, leads to limited success of PS interferometry

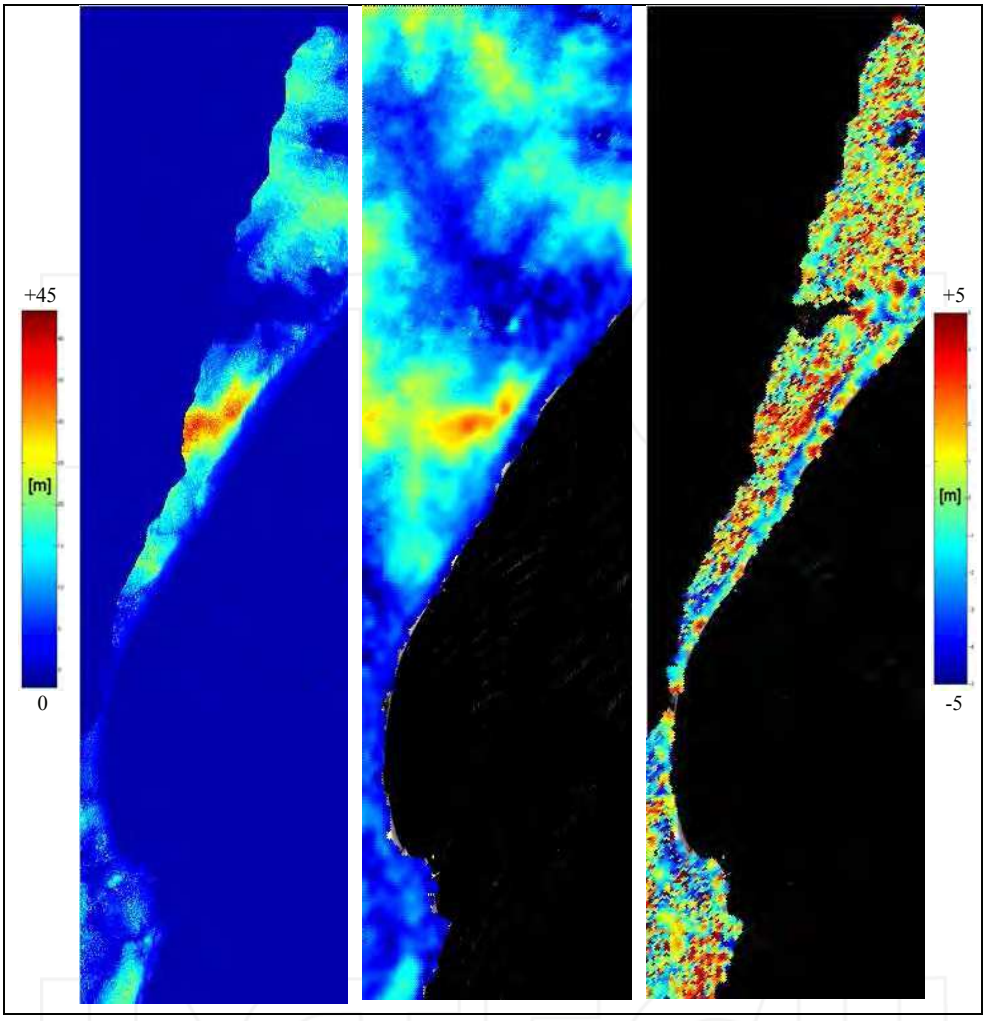

Fig. 9. DSM obtained by LiDAR (left), by Multi-Interferogram InSAR (centre) and map of the LiDAR-InSAR elevation differences (right). Colorbars shown for elevation (left) and errors (right). Minimum standard deviation of 2.56 m is a good estimate of InSAR topography accuracy in the whole area.

As for merge of the very-high resolution LiDAR, and moderate-to-high resolution other spatial data, it is worth recalling that raw data coming from the LiDAR airborne acquisition are in dual form, "first pulse" and "last pulse". First-pulses, allow mapping the reflecting envelope surface and give rise to DSM; whereas the last-pulses subset, the DGM or "ground", is constituted of rays bouncing back from the ground after crossing void spaces in the canopy.

The generic definition of "DEM" (Digital Elevation Model), applies to elevation of terrain referred to bare-Earth without vegetation and/or buildings (Figure 5-right). In order to deal

with LiDAR and InSAR data at once, conversely, we had to split models into DGM ("ground") and DSM ("surface"). Definitely, DGM refers only to LiDAR, whereas DSM (Figures 5-left and 8) - that envelopes the whole of reflecting structures above the Earth's surface - refers also to RaDAR. Consequently, a comparison between different results obtained in the East - by space and RaDAR - and in the West and South - by air and LiDAR - can be performed only on Digital Surface Models.

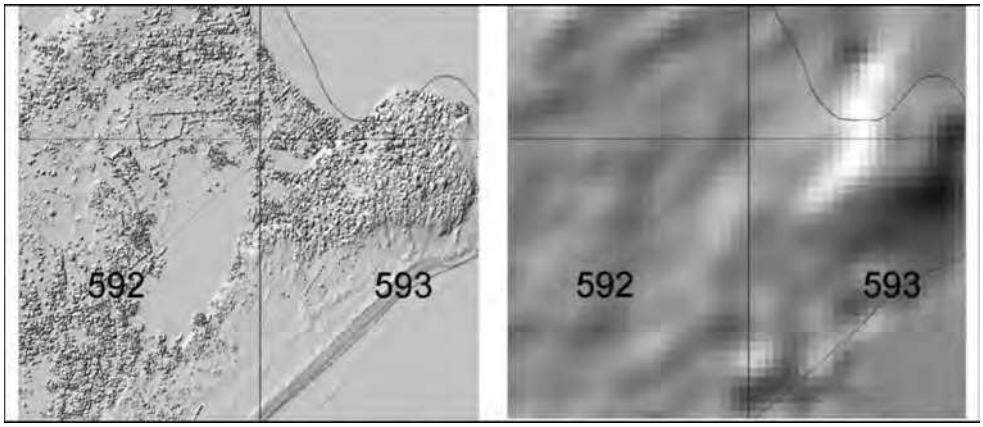

Fig. 10. Difference in resolution of Digital Surface Models of Arugam Bay, southeastern Sri Lanka, obtained by LiDAR (left) and Synthetic Aperture Radar (right). The shaded relief images show the first-pulse, 1-meter LiDAR shaded relief DSM (left) and its equivalent from the 20-meter PS-InSAR™ interferometric DEM. The shoreline of the official cartography 1/50'000 is also shown (gray line).

Comparison, done over the LiDAR-InSAR, DSM overlap area of Arugam Bay in the southeast (see Figures 9 and 10) leads to a satisfactory, least standard deviation value of 2.56 meters.
It is worth noting, however, that such comparison is carried out on products displaying a two-order of magnitude difference in ground resolution, that is, 1 square meter per pixel for LiDAR, vs. 400 square meters for InSAR.

5. Results and products

Raw data leading to the construction of precise 3-D models of the explored coastal areas of Sri Lanka, came from spaceborne Synthetic Aperture RaDAR (SAR) and airborne LiDAR surveying.
Both types of data data were post-processed, to remove errors and fill by resampling and interpolation voids arising from acquisition, and to transform clouds of points in (X, Y, Z) in a grid of X-Y evenly spaced points endowed with the inherent Z elevation fields. Information that can be extracted from LiDAR is dual: "first pulse" and "last pulse".
First pulses relate to Laser beam reflections from the external envelope of objects (canopy, roofs, electric wires, etc.), whereas last detectable pulses in a Laser beam reflection sequence can be associated to the last reflector, that is, bare Earth. Such dual LiDAR (Laser Scanner)

datasets, give rise to two, 3-D cartographic products (Figure 5): Digital Ground Model (DGM) and Digital Surface Model (DSM) , to be used alone or in combination.
DGM represents the bare-Earth elevation cleaned of vegetation and manufacts, whereas DSM represent the elevation of LIDAR first pulses, including manufacts. DGM is suitable for mapping the water penetration in vegetated areas, provided with smooth topography and little or nil 3-D manufacts.
DSM is indicated for detailed inundation mapping in urban areas since it contains 3-D footprints of manufacts, that are of utmost relevance in risk assessment if such vulnerable elements are in the reach of tsunami or storm surge generated flooding.
Conversely, spaceborne RaDAR data allow creating one product – DSM - Due to much longer wavelength (~$6*10^{-2}$ metres for Radar against ~$1*10^{-6}$ metres for LiDAR) and pixel size (~500 m^2 for Radar against ~1 m^2 for LiDAR). However, spaceborne DSM obtained by PS-InSAR™ RaDAR interferometry, are accurate enough to approximate realistically the terrain in areas with sparse or nil vegetation.
Post-processed LiDAR products keep a horizontal resolution of 1 meter, displaying an accuracy in elevation (pseudo-vertical) better than 30 cm.
The interferometric RaDAR product presents a horizontal resolution of 20 meters, an average vertical precision of ±3 meters, with a resolution in elevation better than 1cm in multi-temporal, differential mode only.
Accounting for the huge data volume, the process of map generation required developing an automated procedure to process the dataset, preserve the surface information, and minimize time consumption. The nearest neighbour interpolation method was used to generate DGMs and DSMs from raw data.
This kind of interpolation method has the property of not extrapolating above or below actual data values coming from input. This has appeared essential, because of (a) the very close spacing of input data points, and (b) the fact that other potential methods (e.g. polynomial functions or kriging) may substantially modify the representation of some terrain attributes like buildings or tree canopy.
LiDAR models were arranged in tiles of 1000 x 1000 x 1 metre (excepting those along the shoreline), for as much as 4600 billion grid points measured in elevation (Baltsavias, 1999; Kraus & Pfeifer, 1998; Axelsson, 2000).
Spaceborne RaDAR Digital Surface Models were arranged in two frames of 1811x3497 and 894x3202 (columns x rows) respectively, with 20-metre spacing of points, allowing for total 2.4 million grid points measured in elevation.

6. Simulations

According to the inter-Government agreement referred to above, the Disaster Management Centre in Colombo was provided also with a few inundation examples (Figures 11 and 12), aimed to demonstrate the procedures for tsunami and/or storm surge scenario building - whose responsibility and exploitation rights stay with the national Authority.

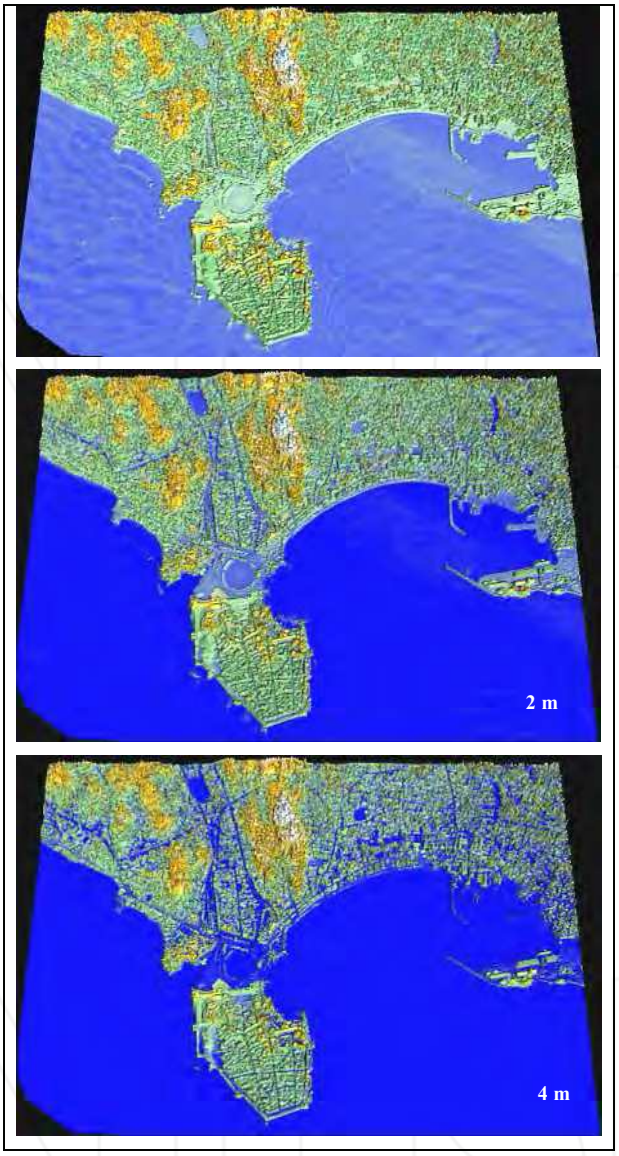

Fig. 11. Shaded relief, Digital Surface Model of the town of Galle, in the Southwest, with static demonstration of flooding simulation by a 2-meter (center) and a 4-meter (bottom) model surge. The synthetic urban flooding scenario shown here, is satisfactorily consistent with field evidence observed at Galle in the aftermath of the event of December 26, 2004. The full wave cut the 17th Century Dutch Fort (bottom) off from mainland, but did not hit the internal streets. This simulation demonstrates that areas allowing safe escape from a 4-meter tsunami, storm surge or tidal wave, can be found and better reached close to the shoreline instead than inland.

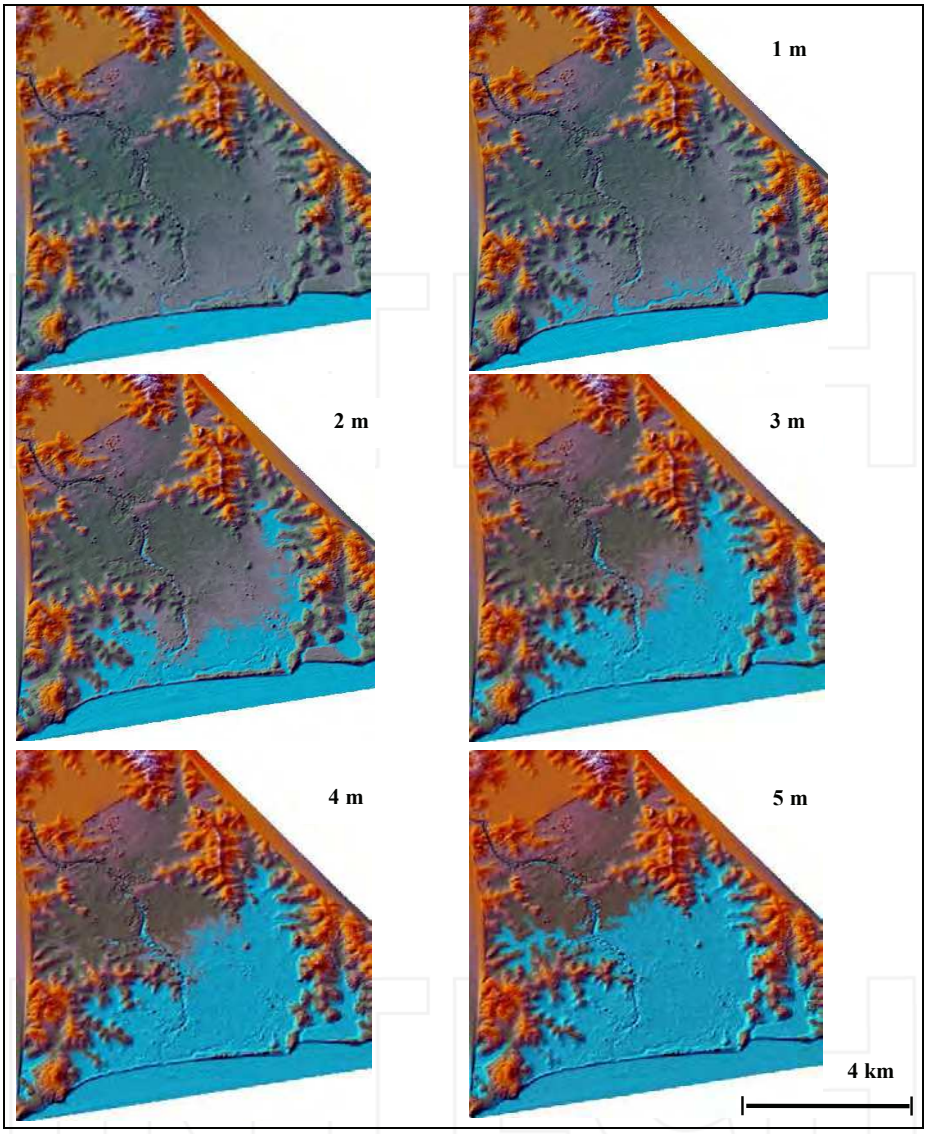

Fig. 12. Shaded relief, Digital Ground Model in the area of Hambantota, southeastern coast, with static flooding simulation by a model surge corresponding to a ca. 5-meter tsunami wave estimated by eye-witnesses and later field investigations. The combination of very low topographic gradient, and presence of lagoons, rivers and ponds close to the shoreline, led to significant inland impact of the incoming wavetrain (over 4 km).

In lack of specific works in scientific literature - that is more focused on the propagation at sea and the impact effects on the sea-shore interface - the demonstrations were carried out following a simplified static approach, consisting in the consecutive piling-up of 1-meter

thick layers. Since the procedure does not account for the significant, dynamic component of tsunami wavetrains, it is probably better suited to storm surges or tidal waves. The sites chosen for demontration are the urban area of Galle - in the southwest - and the area of Hambantota, in the southeast.
Galle (Figure 11) and the surrounding coast were the site of major damage and casualty (more than 4'000), engendered by a relatively small wave height reported in the order of 4 meters. In Hambantota, (Figure 12) the impacting tsunami wave was reportedly steeper, higher (5-6 meters, according to eye-witnesses) and penetrating the coast by a few kilometers. Such significant water ingression is explained by the combination of little topographic gradient over ca. 4-5 kilometers, and presence of large lagoons (at the foot of Hambantota itself), ponds, and rivers. As in Galle with a 4-meter wave, in Hambantota the simulation with a 5-meter wave satisfactorily fits the observed extent of flooding.

7. Conclusions

In the broad aftermath of the Sri Lanka tsunami disaster, the stack of synoptic procedures and remote sensing techniques chosen for satisfying the urgent needs of the User, presented the undebated advantage of : (a) allowing to start the work immediately, (b) without relying upon ground logistics until the onset of the air campaign, (c) minimizing the duration of the work on spot, (d) covering fast - and at an otherwise unreacheable resolution - large portions of a difficult-to-penetrate territory, (e) keeping the work sustainable and, overall, (f) allowing to carry out the work. This combination of airborne and spaceborne techniques was, and is ready-to-use worldwide, and the techniques for flooding simulation and scenario building, can be chosen at whatever level of complexity - choosing preferably robustness.
It is also worth noting further that the new generation of metric resolution, X-band Radar satellite constellations (as TerraSAR-X and Cosmo-SkyMED), may allow creating LiDAR-like products avoiding the air work on spot. Conversely, much is missing on the standpoint of Infra-Red observation, that has currently become poor and poorly resoluted in terms of SWIR spectral resolution (necessary for vegetation and bare soils applications). Whatever the choice of the platform, however, the technique combination holds valid and robust for further applications. In conclusion, the HyperDEM products were handed over by the Ambassador of Italy in Sri Lanka to the Minister for Disaster Management and Humanitarian Affairs, on 7th December 2006, in Colombo, Sri Lanka.

Acknowledgements

The project HyperDEM on tsunami preparedness in Sri Lanka was funded by the Italian Ministry of Foreign Affairs, Directorate General for Cooperation, and promoted by the Sri Lanka Government, Ministry of Disaster Management and Humanitarian Affairs, and Ministry of Science and Technology. Its carrying out overseas involved more than 20 scientists, engineers and technicians, guided by Franco Coren, Giuliano Savio, Barbara Hirn, Michela Vellico, Paolo Sterzai and Gianluca Calabretta, under the coordination of the author. Field effort and post-processing of a ca. 3-TeraByte data gather benefited of the support of three technological partners, owning and exploiting 7 international patents involved in the whole process (HeliOGS Consortium in airborne acquisition and LiDAR; IES Consulting - Intelligence for Environment and Security, in hyperspectral and multispectral data processing; TRE-Telerilevamento Europa in RaDAR interferometry and PS-InSAR™).

Pre/post-tsunami, very high-resolution multispectral QuickBird scenes were granted by the Pacific Disaster Center of Maui, Hawaii. The whole work was supported by the Sri Lankan Air Force, the Disaster Management Centre, Sri Lankan Airlines and the pilots of Air Taxi, and the Italian Embassy in Colombo. Special acknowledgements are due to Amb. Salvatore Zotta and Maj. Gen. Gamini Hettiarachchi, who allowed solving any criticality incurred when designing, launching and carrying out HyperDEM.

8. References

Axelsson, P. (2000), DEM Generation from Laser Scanner data Using Adaptive TIN Models, International Archives of Photogrammetry and Remote Sensing, Vol. XXXIII, B4. Amsterdam.

Baltsavias, E.P. (1999), Airborne laser scanning: basic relations and formulas. ISPRS Jour. Photogramm. Rem. Sens., 54, 199-214.

Colesanti C., Ferretti A., Ferrucci F., Prati C., and F. Rocca (2000). Monitoring Known Seismic Faults Using the Permanent Scatterers (PS) Technique, Procs. IEEE International Geoscience and Remote Sensing Symposium - IGARSS 2000 (Honolulu, USA, 24-28 July), 5, 2221-2223.

Eisner R.K., Borrero J.C., and C.E. Synolakis (2001). Inundation maps for the State of California. Procs. ITS-International Tsunami Symposium 2001 and NTHMP Review Session (Seattle, USA, 7-10 August); R-4, 67-81.

Ferretti, A., C. Prati, and F. Rocca (1999), Multibaseline InSAR DEM Reconstruction: the Wavelet Approach, IEEE Trans. Geosci. Rem. Sens., 37, 2; 705-715.

Ferretti, A., C. Prati, and F. Rocca (2001), Permanent scatterers in SAR interferometry, IEEE Trans. Geosci. Rem. Sens., 39, 1; 1528-1530.

Ferrucci, F., and B. Hirn (2005), An automated method for detecting and mapping, particularly for areas without vegetation; International Patent, PCT WO2005/005926A1, published: January 26, 2005.

Geist, E.L., V.V. Titov, D. Arcas, F.F. Pollitz, and S.L. Bilek (2007): Implications of the 26 December 2004 Sumatra-Andaman Earthquake on tsunami forecast and assessment models for great subduction-zone earthquakes. Bull. Seism. Soc. of Am., 97, 1A; 249-270.

Gregg, C.E.; Houghton, B.F.; Paton, D; Johnston, D.M., Swanson, D., and B. A. Yanagi,(2007). Tsunami Warnings: Understanding in Hawafi. Nat. Hazards 40:71-87.

Hammack, J. L. (1973), A Note on Tsunamis: Their Generation and Propagation in an Ocean of Uniform Depth, J. Fluid Mech., 60, 769-799.

Hirn, B., and F. Ferrucci (2005). MYME2: a Multi-Payload Integrated Procedure for the Automated, High-Resolution Remote Sensing of Burn Scars. Procs. IEEE International Geoscience and Remote Sensing Symposium - IGARSS 2005, (Seoul, South Korea, 25-29 July) paper no. 20238; 5721-5724.

Kraus, K., and N. Pfeifer (1998), Determination of Terrain Models in wooded areas with Airborne laser Scanner data, ISPRS Jour. Photogramm. Rem. Sens., 53, 4: 193-203.

Lander, J.F., P.A. Lockridge, and M.J. Kozuch (1993). West coast of the United States 1806-1992. NGDC Key to Geophysical Record Documentation 29, NOAA, 242 pp.

Leblond, P. H. and Mysak, L. A. (1978) Waves in the Ocean (Elsevier Scientific Publishing Company.

Liu P.L.F., Lynett P., Fernando H., Jaffe B.E., Fritz H., Higman B., Morton R., Goff J., and C Synolakis (2005). Observations by the International Tsunami Survey Team in Sri Lanka. Science; 308, 5728, p. 1595. DOI: 10.1126/science.1110730

Monti Guarnieri, and A. and Ferretti (2000). Visibility of Permanent Scatters by ScanSAR. Procs. EUSAR 2000 (Munich, Germany, May 23-25), 725-728.

Monti Guarnieri, and Y-L. Desnos (1999), Optimizing performances of the ENVISAT ASAR ScanSAR modes. Procs. IEEE International Geoscience and Remote Sensing Symposium - IGARSS 1999 (Hamburg, Germany, June 28-July 2), 1758-1760.

Oppenheimer, D., Beroza, G., Carver, G., Dengler, L., Eaton, L., Gee, L., González, F., Jayko, A., Li, W. H., Lisowski, M., Magee, M., Marshall, G., Murray, M., McPherson, R., Romanowicz, B., Satake, K., Simpson, R., Somerville, P., Stein, R. and Valentine, D. (1993), The Cape Mendocino, California, Earthquakes of April 1992: Subduction at the Triple Junction, Science, 261, 433-438.

Prati, C., F. Rocca, A. Monti Guarnieri (1994), Topographic capabilities of SAR exemplified with ERS-1. Geo Information System, 7, 1; 17-23.

Priest G.R., Baptista A.M., Myers E.P.III, and R.A. Kampahaus (2001). Tsunami hazard assessment in Oregon. Procs. ITS-International Tsunami Symposium 2001 and NTHMP Review Session (Seattle, USA, 7-10 August) ; R-3, 55-65.

Satake, K., Bourgeois, J., Abe, K., Abe, K., Tsuji, Y., Imamura, F., Iio, Y., Katao, H., Noguera, E. and Estrada, F. (1993), Tsunami Field Survey of the 1992 Nicaragua Earthquake, Eos, Trans., Am. Geophys. Union, pp. 74, 145 and 156-157.

Sibuet, J-C., Rangin, C., Le Pichon, X., Singh, S., Cattaneo, A., Graindorge, D., Klingelhoefer, F., Lin, J-Y., Malod, J., Maury, T., Schneider, J-L., Sultan, N., Umber, M., Yamaguchi, H., and the "Sumatra aftershocks" team (2007). 26th December 2004 great Sumatra-Andaman earthquake: Co-seismic and Post-seismic motions in northern Sumatra; Earth Plan. Sci. Lett., 263, 1-2, 88-103.

Tinti, S., A. Armigliato, A. Manucci, G. Pagnoni, and F. Zaniboni (2005), Landslides and tsunamis of 30th December 2002 at Stromboli, Italy: numerical simulations, Boll. Geofis. Teor. Appl., 46, 153-168.

Tinti, S., A. Armigliato, A. Manucci, G. Pagnoni, F. Zaniboni, A.C. Yalginer, and Y. Altinok (2006), The generating mechanism of the August 17, 1999 Izmit Bay (Turkey) tsunami: Regional (tectonic) and local (mass instabilities) causes; Marine Geol., 225, 311-330.

Titov, V.V., and C.E. Synolakis (1998). Numerical modeling of tidal wave runup. J. Waterw. Port Coast. Ocean Eng., 124, 4; 157-171.

Venturato, A.J., D. Arcas, V.V. Titov, H.O. Mofjeld, C.C. Chamberlin, and F.I. Gonzalez (2007): Tacoma, Washington, tsunami hazard mapping project: Modeling tsunami inundation from Tacoma and Seattle fault earthquakes. NOAA Tech. Memo. OAR PMEL-132, 23pp.

Weiss R., Wünnemann K., and H. Bahlburg (2006). Numerical modelling of generation, propagation and run-up of tsunamis caused by oceanic impacts: model strategy and technical solutions. Geophys. Jour. Int.; 167, 1; 77-88.

Whitmore, P.M. (1993), Expected Tsunami Amplitudes and Currents along the North American Coast for Cascadia Subduction Zone Earthquakes, Nat. Hazards, 8, 59-73.

Wiegel, R. L. (1976). Tsunamis. In: Seismic Risk and Engineering Decisions; C. Lomnitz and E. Rosenblueth, eds.; Elsevier Scientific Publishing Co., Amsterdam (NL) 225-286.

Geoscience and Remote Sensing New Achievements

Edited by Pasquale Imperatore and Daniele Riccio

ISBN 978-953-7619-97-8
Hard cover, 508 pages
Publisher InTech
Published online 01, February, 2010
Published in print edition February, 2010

Our planet is nowadays continuously monitored by powerful remote sensors operating in wide portions of the electromagnetic spectrum. Our capability of acquiring detailed information on the environment has been revolutionized by revealing its inner structure, morphology and dynamical changes. The way we now observe and study the evolution of the Earth's status has even radically influenced our perception and conception of the world we live in. The aim of this book is to bring together contributions from experts to present new research results and prospects of the future developments in the area of geosciences and remote sensing; emerging research directions are discussed. The volume consists of twenty-six chapters, encompassing both theoretical aspects and application-oriented studies. An unfolding perspective on various current trends in this extremely rich area is offered. The book chapters can be categorized along different perspectives, among others, use of active or passive sensors, employed technologies and configurations, considered scenario on the Earth, scientific research area involved in the studies.

How to reference

In order to correctly reference this scholarly work, feel free to copy and paste the following:

Fabrizio Ferrucci (2010). Integration of High-Resolution, Active and Passive Remote Sensing in Support to Tsunami Preparedness and Contingency Planning, Geoscience and Remote Sensing New Achievements, Pasquale Imperatore and Daniele Riccio (Ed.), ISBN: 978-953-7619-97-8, InTech, Available from: http://www.intechopen.com/books/geoscience-and-remote-sensing-new-achievements/integration-of-high-resolution-active-and-passive-remote-sensing-in-support-to-tsunami-preparedness-

INTECH
open science | open minds

InTech Europe
University Campus STeP Ri
Slavka Krautzeka 83/A
51000 Rijeka, Croatia
Phone: +385 (51) 770 447
Fax: +385 (51) 686 166
www.intechopen.com

InTech China
Unit 405, Office Block, Hotel Equatorial Shanghai
No.65, Yan An Road (West), Shanghai, 200040, China
中国上海市延安西路65号上海国际贵都大饭店办公楼405单元
Phone: +86-21-62489820
Fax: +86-21-62489821